Coupling of Focal Mechanism with finite Difference Wave Propagation

in Rotated Staggered Grid

Junlun LI

Department of Earth, Atmospheric and Planetary Sciences, MIT

Introduction

Finite difference scheme has been widely used to solve elastic wave propagation in heterogeneous and layered media. Traditionally, staggered grid scheme is used for differencing the equations of Newton's Motions Law and Generalized Hook's Law describing the elastic wave propagation. In the two dimensional case, the equations can be expressed as follow:

$$\rho \frac{\partial v_x}{\partial t} = \frac{\partial \tau_{xx}}{\partial x} + \frac{\partial \tau_{xz}}{\partial z}$$
$$\rho \frac{\partial v_z}{\partial t} = \frac{\partial \tau_{xz}}{\partial x} + \frac{\partial \tau_{zz}}{\partial z}$$
$$\frac{\partial \tau_{xx}}{\partial t} = (\lambda + 2\mu) \frac{\partial v_x}{\partial x} + \lambda \frac{\partial v_z}{\partial z}$$
$$\frac{\partial \tau_{zz}}{\partial t} = \lambda \frac{\partial v_x}{\partial x} + (\lambda + 2\mu) \frac{\partial v_z}{\partial z}$$
$$\frac{\partial \tau_{xz}}{\partial t} = \mu (\frac{\partial v_x}{\partial z} + \frac{\partial v_z}{\partial x})$$

Where v_x, v_z is velocity component, τ_{ij} is stress component, ρ is density, λ, μ are Lame constant. For traditional staggered grid method, we would discretize the above equations as in the following scheme:

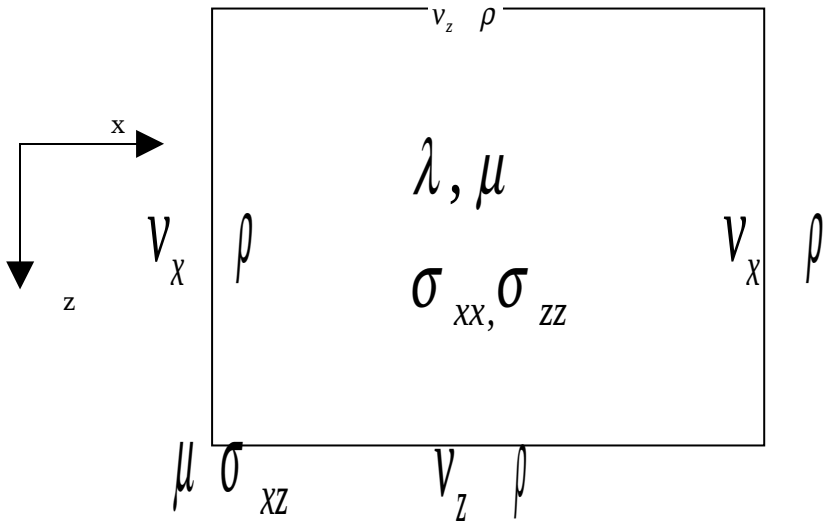

Fig. 1. Traditional Staggered grid scheme

By placing as above, the velocity components and stress components are in staggered grids. However, when we update velocity components v_x and v_z and shear stress σ_{xz}, we have to use averaged density and shear modulus. For density we simply use arithmetic average and it is fine when wave transmitted from solid into vacuum or some medium with very low density. However, when we average shear modulus μ, we should use harmonic averaging:

$$\frac{4}{\mu(i-\frac{1}{2}, j-\frac{1}{2})} = \frac{1}{\mu(i, j)} + \frac{1}{\mu(i-1, j)} + \frac{1}{\mu(i-1, j-1)} + \frac{1}{\mu(i, j-1)}$$

Therefore, when wave transmitted from solid into some medium with zero or very small shear modulus, at the boundary point the equation will blow up.

In order to solve this problem, Saenger et. al. proposed another approach called

rotated staggered grid. Their basic idea is to rotate the coordinate system that all the stresses are located at the center of the cell. In doing so, when stresses are updated, no averaging among the neighboring points is needed. Their algorithm can be expressed in the following plot:

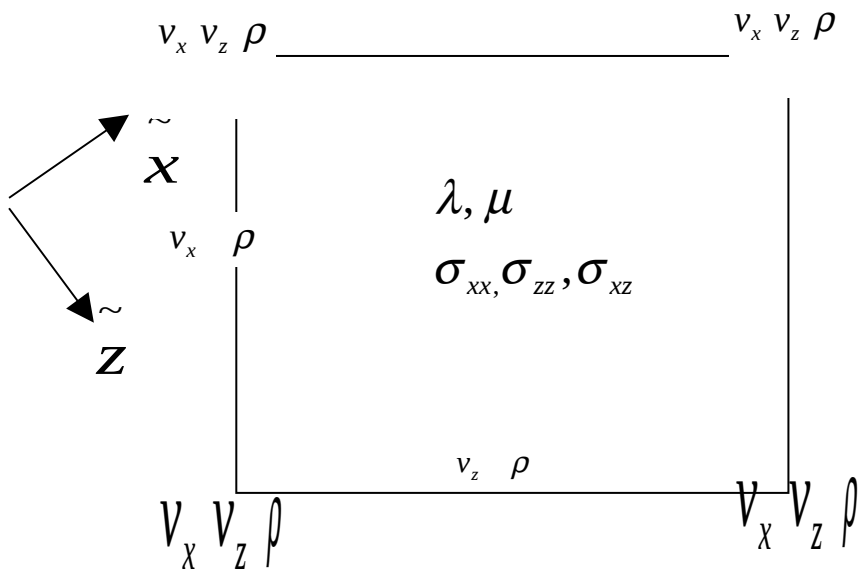

Fig. 2. Rotated staggered grid scheme

This new rotated staggered grid can be related to the traditional staggered grid with the following coordinate transforms:

$$\tilde{z} = \frac{\Delta x}{\Delta r} x + \frac{\Delta z}{\Delta r} z$$
$$\tilde{x} = \frac{\Delta x}{\Delta r} x - \frac{\Delta z}{\Delta r} z$$
$$\Delta r = \sqrt{\Delta z^2 + \Delta x^2}$$

In traditional coordinate system, we define the following 2nd order operator as:

$$D_x u(x,z,t) = \frac{1}{\Delta x}\left[u(x+\frac{\Delta x}{2},z,t) - u(x-\frac{\Delta x}{2},z,t)\right]$$
$$D_z u(x,z,t) = \frac{1}{\Delta x}\left[u(x,z+\frac{\Delta z}{2},t) - u(x,z-\frac{\Delta z}{2},t)\right]$$

Then we can get the 2nd order operator in the new rotated coordinate system as:

$$D_{\tilde{x}} u(x,z,t) = \frac{1}{\Delta x}\left[u(x+\frac{\Delta x}{2},z-\frac{\Delta z}{2},t) - u(x-\frac{\Delta x}{2},z+\frac{\Delta z}{2},t)\right]$$
$$D_{\tilde{z}} u(x,z,t) = \frac{1}{\Delta x}\left[u(x+\frac{\Delta x}{2},z+\frac{\Delta z}{2},t) - u(x-\frac{\Delta x}{2},z-\frac{\Delta z}{2},t)\right]$$

Then we transform them back into the traditional coordinate system:

$$\frac{\partial}{\partial x}u(x,z,t) \approx \frac{\Delta r}{2\Delta z}\left[D_{\tilde{x}} u(x,z,t) + D_{\tilde{z}} u(x,z,t)\right]$$
$$\frac{\partial}{\partial z}u(x,z,t) \approx \frac{\Delta r}{2\Delta z}\left[-D_{\tilde{x}} u(x,z,t) + D_{\tilde{z}} u(x,z,t)\right]$$

By doing so, we can obtain a new set of discretized equations for describing the elastic wave propagation.

Thanks to Cruz-Atienza etc., we could have an easier insight into this coordinate rotation approach. Besides the above expression of algorithm, we could define

$$D_x(f_{ij}) = \frac{1}{2h}(f_{i+1/2,j+1/2} - f_{i-1/2,j-1/2} + f_{i+1/2,j-1/2} - f_{i-1/2,j+1/2})$$
$$D_z(f_{ij}) = \frac{1}{2h}(f_{i+1/2,j+1/2} - f_{i-1/2,j-1/2} - f_{i+1/2,j-1/2} + f_{i-1/2,j+1/2})$$

And if we discretize the original differential equations by these differencing operators, we could have the same difference equations as derived from above.

Implementations

1). Air Wave Propagation

The whole codes are written in Matlab. Perfectly Matched Layers (PML) with 40 grids in thickness are placed on the four boundaries. For simulation, we use grid size dh=2 m. The whole area is 240x300 grids. There are two layers in this model: from grid 1 to 60 is air, which has a density of 1.292 kg/m^3, Vp=340 m/s, and shear modulus u=0; from grid 61 to 300 is rock, which has a density of 3000 kg/m^3, Vp=3464 m/s, Vs =2000 m/s. From the density, Vp and Vs, we can calculate the Lame constants. Although we now only deal with two layers, the numerical scheme actually can handle heterogeneous media as later we will see.

For simulation wave propagation, an isotropic explosion source is used, which is added to stresses $\sigma_{xx,}\sigma_{zz}$ within a 3x3 square area. As pointed out by Cruz-Atienza etc., this scheme could be a better approximation of point source than just using one single point. The source center is located at grid (120, 100). The source time function is a Ricker wavelet, which in time domain can be expressed as below:

$$\sigma_{xx,}\sigma_{zz} = A(1 - a^2t^2)\exp(-a^2t^2/2)$$

Where A is amplitude, a= $f_0 \cdot \sqrt{2}\pi$, f_0 is the central frequency. The wavelet is demonstrated below:

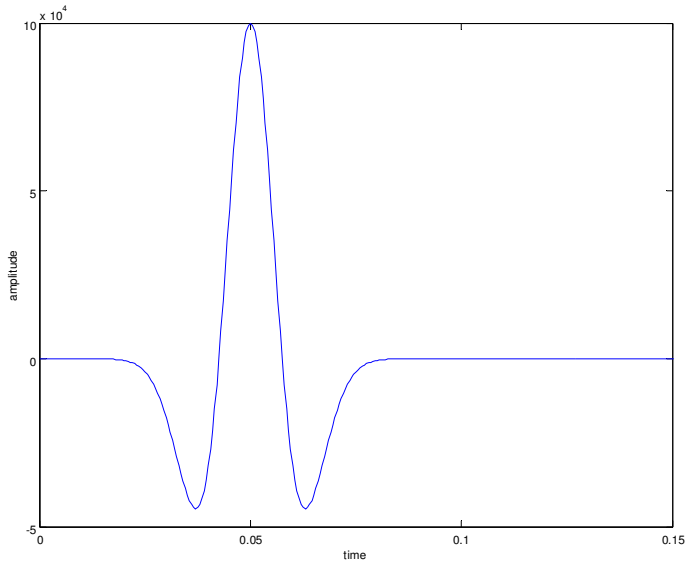

Fig. 3. Wavelet for Simulating Air Wave propagation

The velocity distributions at t=0.120 s are plotted as below

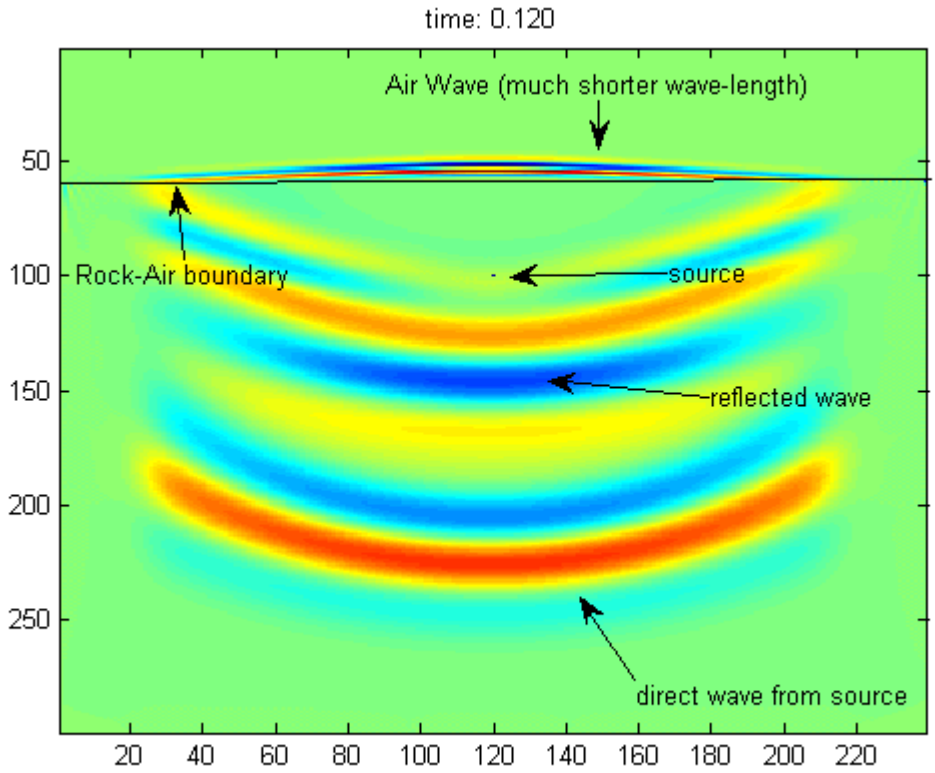

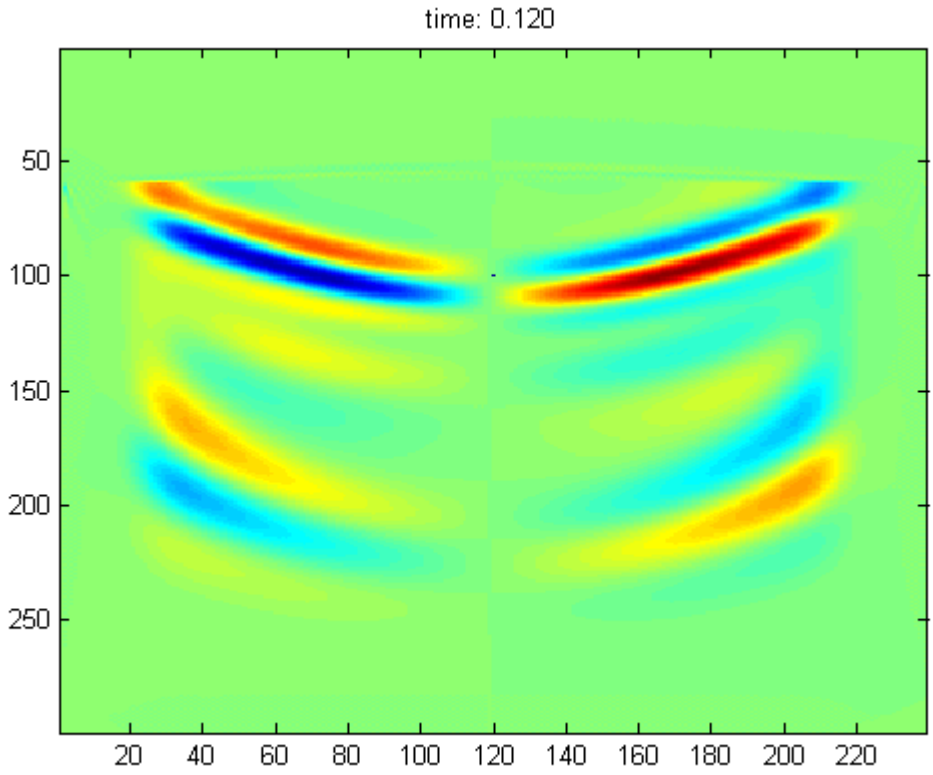

Fig. 4. Air Wave Propagation: first row is Vz and second row is Vx

From the figures above we can clearly see that this numerical scheme works well for high contrast media. The wave transmitted into air can be correctly modeled. No Vx component exists in the air as shear wave can not propagate in the air, whose shear modulus u is zero.

One thing should be noticed in the implementations of this paper is that we flip the source time function by π. Due to possible different definition in coordinate system, or possible mistakes in staggered grid rotation or Matlab index usage, we find the phases in our results should be reversed by π to match various benchmark tests. This reverse is applied in source time functions in this paper.

2). Single Arbitrarily Oriented Fault Source

Realistic seismic fault is a finite length rupture, ranging from hundreds of meters to hundreds of kilometers. Traditionally, people would use single point source to approximate a fault if observation point is far enough, e.g., tens of times of the fault length away from the fault. However, for a large seismic fault like San Andreas, we should use finite length fault for modeling. In order to model finite length, arbitrarily oriented fault, we first model a single point, arbitrarily oriented “fault”.

Fig. 5 . San Andreas Fault

Source: http://www.physics.unlv.edu/~jeffery/astro/earth/geology/plate/usgs_020_sanandreas.gif

After Cruz-Atienza etc., we model this problem as follow:

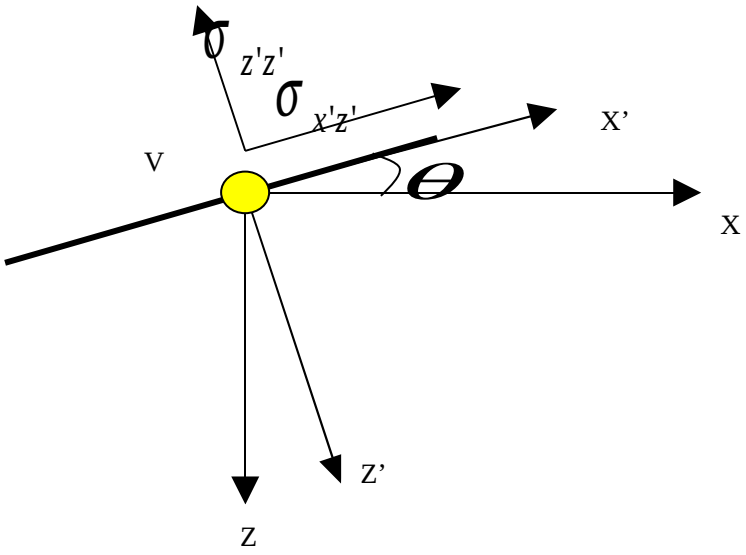

Fig. 6. Local and Global Coordinate for Oriented Single Point Fault

The fault point is rotated by θ from horizontal direction. The fault is rupturing in finite speed V thus it has shear and normal stress $\sigma_{x'z'}$ $\sigma_{z'z'}$ in local X'-Z' coordinate system. However, our numerical scheme is implemented in X-Y coordinate system, thus we have to project the fault stresses into our numerical coordinate by the following transform:

$$\begin{bmatrix} \sigma_{xx} & \sigma_{xz} \\ \sigma_{zx} & \sigma_{zz} \end{bmatrix} = \begin{bmatrix} \cos\theta & -\sin\theta \\ \sin\theta & \cos\theta \end{bmatrix} \begin{bmatrix} \sigma_{x'x'} & \sigma_{x'z'} \\ \sigma_{z'x'} & \sigma_{z'z'} \end{bmatrix} \begin{bmatrix} \cos\theta & \sin\theta \\ -\sin\theta & \cos\theta \end{bmatrix}$$

In our simulation, we assume there is no volume change, thus normal stress $\sigma_{z'z'}$ equal to zero and we only have shear stress $\sigma_{x'z'}$. In order to simulate the true earthquake, we use the following tanh time function source, which in many cases is a good low-pass filtered approximation of realistic earthquake rupturing progress. The function is defined

as:

$$F = \frac{1}{2} * t_o * (1 - \tanh(\frac{t}{t_0})^2)$$

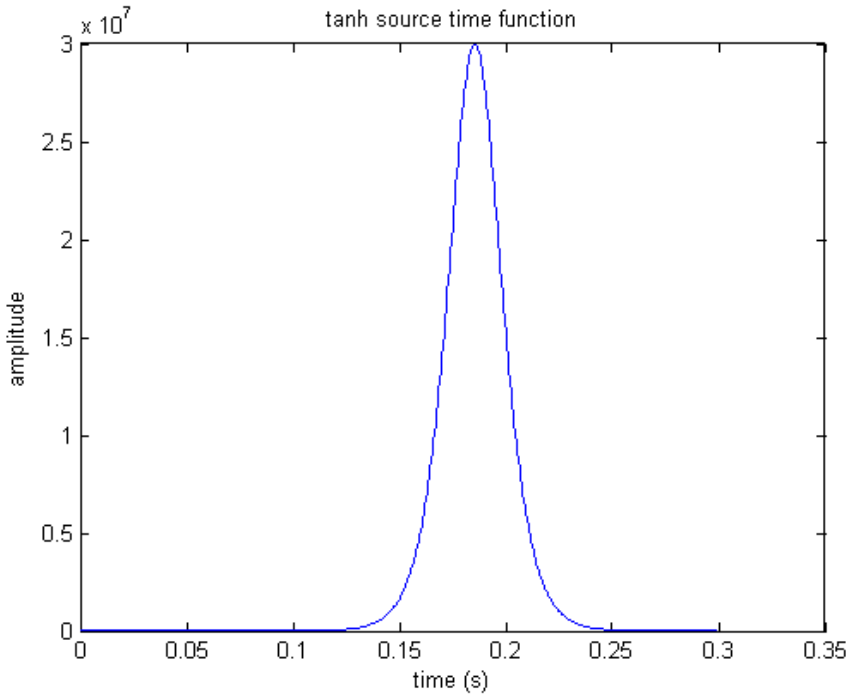

Fig. 7. Tanh source time function

We compare a horizontally oriented source and a 30° oriented source in a 240 by 240 square area with Perfectly Matched Layer absorption boundaries. In the interior area, we use Rotated Staggered Grid as mentioned before, but in the PML area we use traditional staggered grid discretization after Marcinkovich etc. for simplicity.

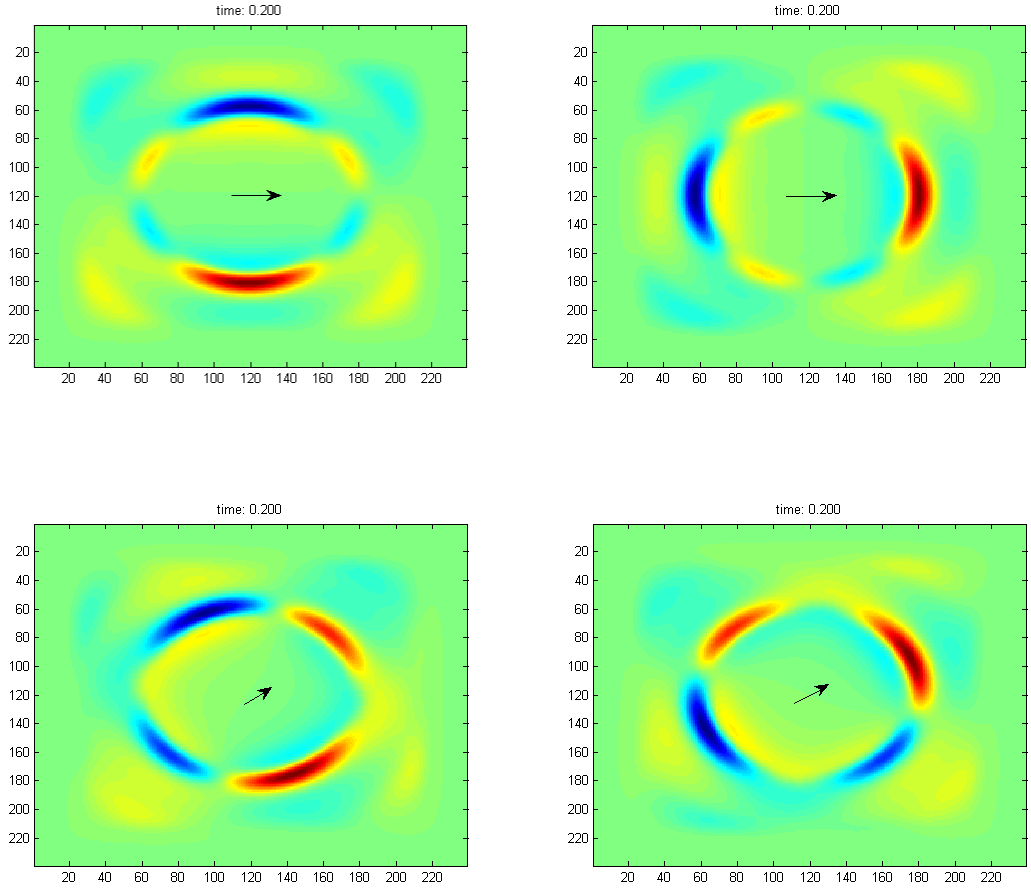

Fig. 8. Velocity field generated by differently oriented single point fault: first row is a horizontal fault and second row is a 30^{o} oriented fault; left column is Vx and right column is Vz

From the comparison between the horizontally oriented point fault and a 30^{o} oriented point fault we can clearly see that velocity fields are rotated by 30^{o}. This implementation of arbitrarily rotated single point fault combined with the following implementation of finite length-finite rupturing speed line fault modeling will provide us the ability to characterize realistic seismic fault of arbitrary geometry.

3). Finite Length-Finite Rupturing Speed line fault

We will model a finite length fault with a rupturing speed of 0.8Vs, where Vs is the shear wave velocity. We use 15 point sources located in line, with a time delay of $\frac{\Delta X}{0.8Vs}$, where ΔX is the distance between two point sources. In another sense, we can consider the fault as a time-delayed phased line array.

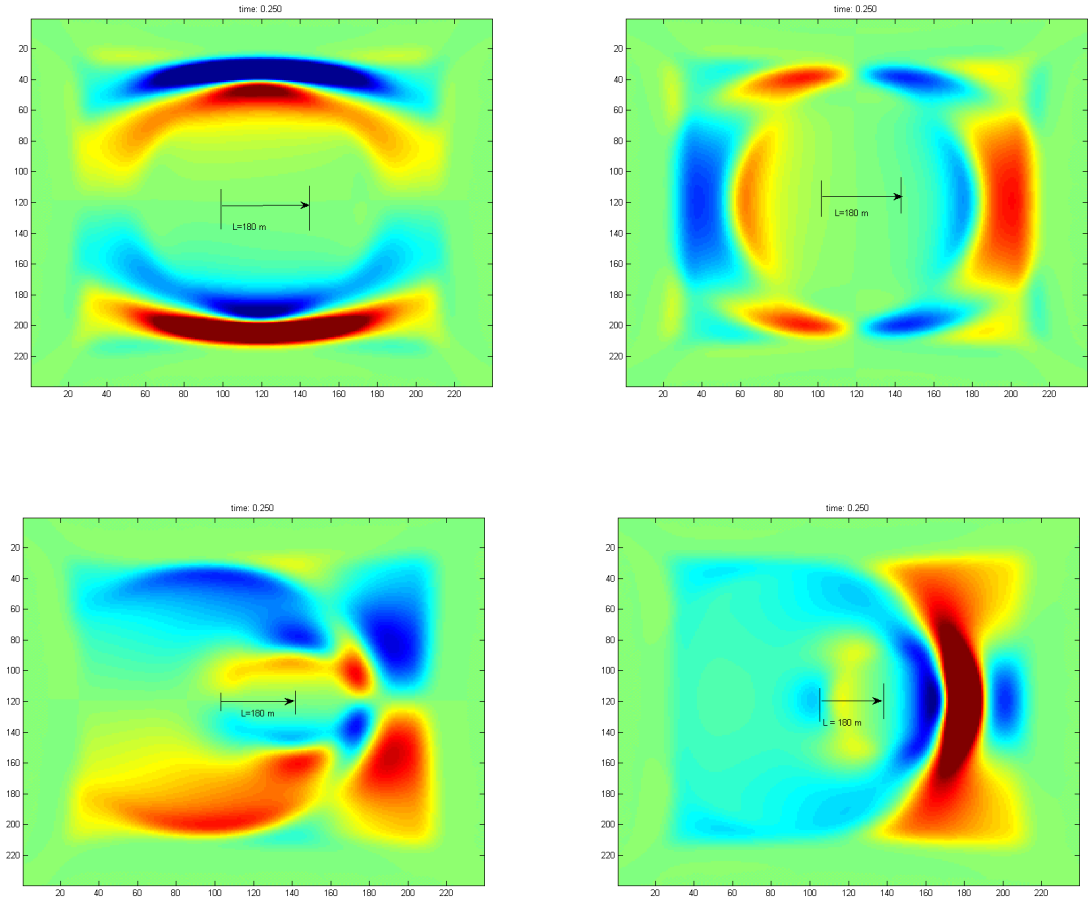

Fig. 9. Radiation pattern by a finite length fault: first row: infinite rupturing speed (simultaneous point sources); second row: finite rupturing fault; left column is Vx and right column is Vz, respectively.

From fig. 9 we can clearly see that the radiation pattern of fault of infinite rupturing speed and finite rupturing speed is quite different. Especially, we can observe obvious Doppler Effect in the finite speed case: the wavefront in the direction of rupture is compressed and thus has very high amplitude, while the wavefront in the reverse direction is elongated and has low amplitude.

In order to understand the problem more clearly, we put two receivers (receiver #1 and #3) at these two opposite directions, each of which is about 60 m away from the ending point of the finite length fault. The results are given in Fig. 10.

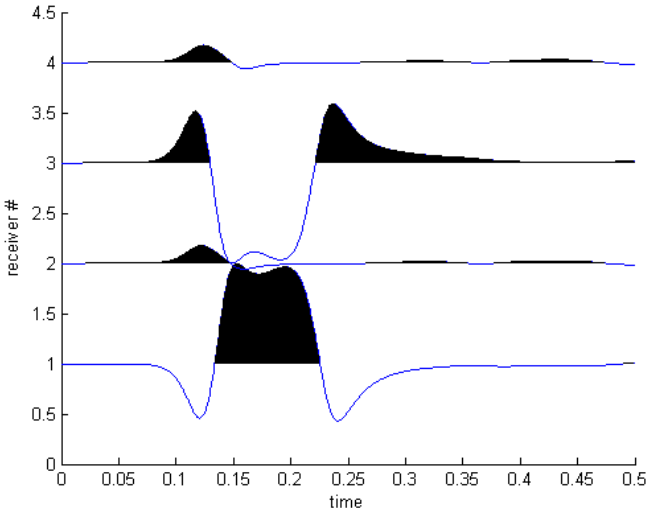

(a)

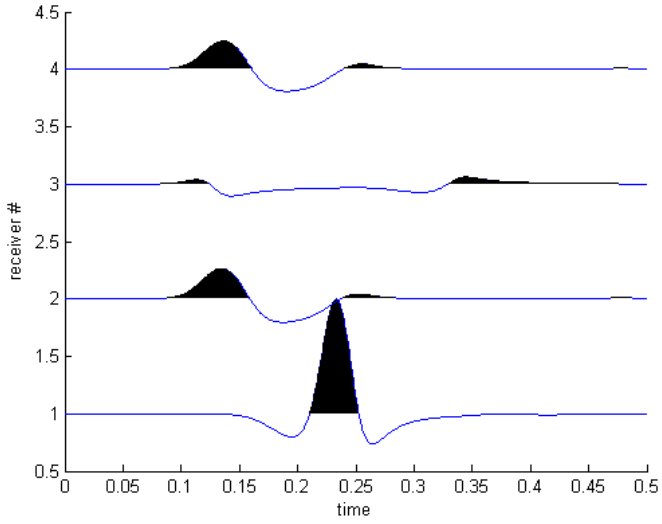

(b)

Fig. 10. seismograms at four different positions. These four seismometers are located at east, north, west and south of the fault. (a). infinite propagation rupture (simultaneous sources); (b). finite propagation rupture (0.8Vs)

From Fig. 10 we can see clearly the changes in the seismogram. In the finite propagation rupture model we can see obvious Doppler Effect: wavefront in the rupture direction is compressed and hence has high amplitude (figure (b), receiver #1), while wavefront in the reverse direction is elongated and hence the amplitude is relatively low. (figure (b), receiver #3). For more straightforward understanding, we can see the signals from receiver #1 and #3 in frequency domain by Fourier transform:

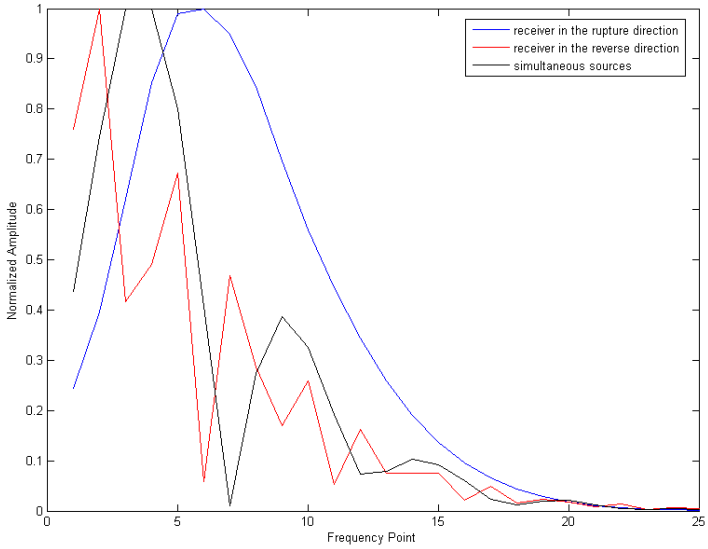

Fig. 11 Fourier transforms of seismograms at seismometer #1 and #3

Compared with the infinite rupturing fault (black line), the finite rupturing fault has an obvious Doppler effect. Frequency of the signal in the rupture direction is shifted higher (blue line), while signal in the reverse direction is shifted lower (red line). The simultaneous case is depicted in the black line.

4). Arbitrarily Shaped and Oriented Fault

Combining the aforementioned two techniques of modeling arbitrarily oriented point fault and time-delayed finite-speed rupturing fault, we could obtain the ability to model any arbitrarily shaped and oriented fault.

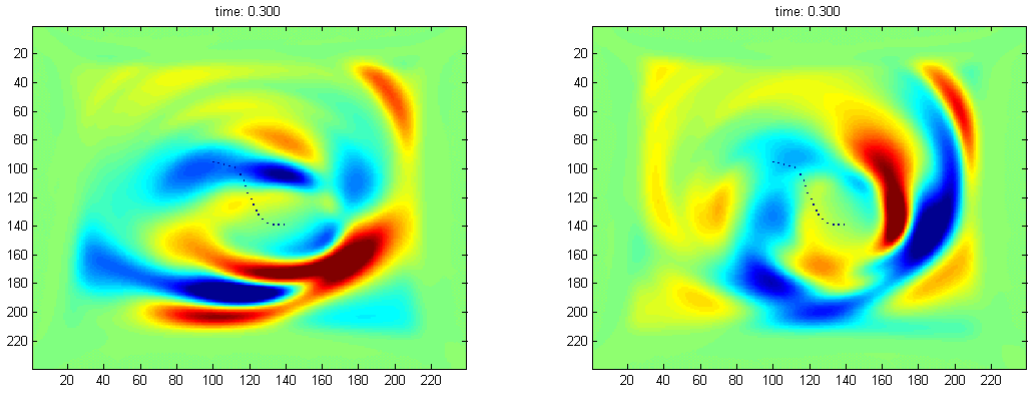

Fig. 12. seismic wave velocity field from complex shaped fault zone; left one is Vx and right one is Vz

Fig. 12 depicts a curved fault zone which propagates in 0.8Vs. The fault zone is depicted in the middle area of the plots by dots. We can clearly see the radiation pattern is changed tremendously. Therefore, we should keep in mind that long fault zone could have a quite different radiation pattern compared with short fault zone.

5). Water Cave scattering

There are many low or high velocity zones underground which would change the path of ray propagation in an obvious sense. For this term project, in order to make things more fun, I would simulate the situation when seismic waves encountering water cave. We should see scattering wave at the boundary due to impedance contrast. Also, we should observe transmission wave through the cave. As wave propagates slowly in water, we could expect wavefront distortion. The simulated water cave in 80 m in diameter and is located as demonstrated in the following figure.

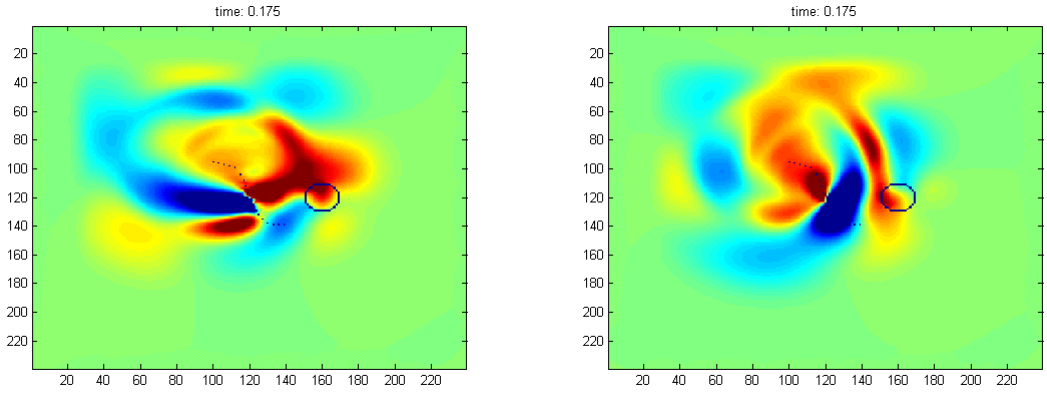

Fig. 13. seismic wave propagation in a domain containing a round water cave

From figure 13 we can clearly see the distortion of wavefront by the water cave, which has a lower velocity and zero shear modulus.

Conclusion

By the inborn discretization natures, the rotated staggered grid method is very suitable for simulating high contrast media, e.g., water and rock or air and rock. When encounter the interface between high contrast media, we do not need to do harmonic averaging, which is going to blow up when divided by zero. In this paper, we model several different interesting situations: 1). Wave propagating into air from rock; 2). arbitrarily oriented single fault source; 3). Finite length-finite rupturing line fault; 4). arbitrarily shaped finite length-finite rupturing fault; 4). Seismic propagation in domain containing water cave. These implementations are bounded with PML layers. With the ability to model more complex structure, we could match theoretical computations with realistic seismic observations better.

Acknowledgement

The author appreciates Yang Zhang for his sincere help and discussion. Also, the author would like to thank B. Seibold, our young and energetic lecturer, for his wonderful teaching in the Spring term in 2008.

References

A. Douglas, J. A. Hudson and R. G. Pearce, Directivity and the Doppler Effect, Bulletin of Seismological Society of America, 78, No.3, pp. 1367-1372

Carey Marcinkovich and Kim Olsen, On the implementation of perfectly matched layers in a three dimensional fourth-order velocity-stress finite difference scheme, J. Geophysical Research, 108, 2003

Erik H. Saenger, Norbert Gold, Serge A. Shapiro, Modeling the propagation of elastic waves using a modified finite difference grid, Wave Motion, Vol. 31, 2000, pp. 77-92

Erik H. Saenger and Thomas Bohlen, Finite-difference modeling of viscoelastic and anisotropic wave propagation using the rotated staggered grid, Geophysics, Vol. 69, No. 2, 2004, pp. 583-591

Seismic Modeling Project, Earth Resources Laboratory (EAPS, MIT)

V. M. Cruz-Atienza and J. Virieux, Dynamic rupture simulation of non-planar faults with a finite-difference approach, Geophys. J. Int. 158, 2004, pp. 939-954

V. M. Cruz-Atienza, J Virieux and Hideo Aochi, 3D finite-difference dynamic-rupture modeling along nonplanar faults, Geophysics, 72, No.5, 2007, pp. 123-137

Notes on Perfectly Matched Layers (PMLs), Steven G. Johnson, 2007